AD-A087 398 MASSACHUSETTS INST OF TECH CAMBRIDGE LAB FOR INFORMA--ETC F/G 10/2
ROBUST CONTROL OF MULTITERMINAL DC/AC SYSTEMS,(U)
AUG 79 N A LEHTOMAKI, S M CHAN, N R SANDELL DOE-ET-78-C-01-3395

UNCLASSIFIED NL

END
DATE FILMED
9 80
DTIC

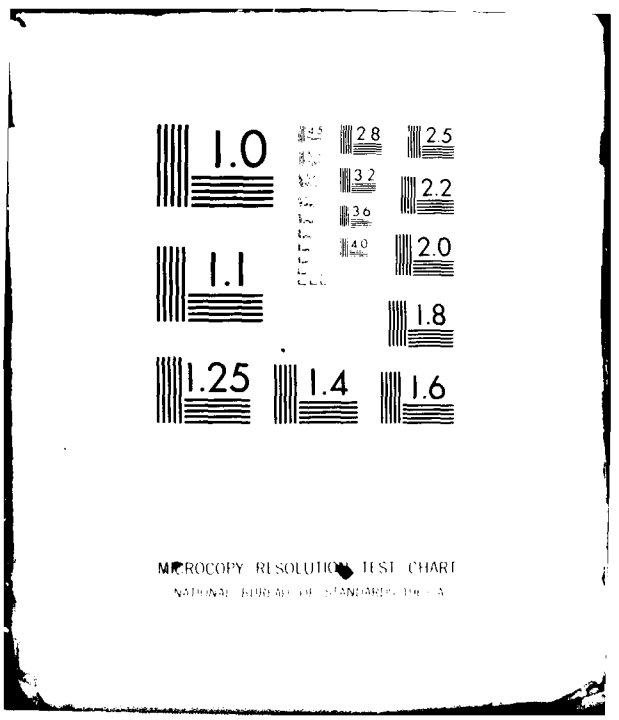
1.0
1.1
1.25
2.8
3.2
3.6
4.0
2.5
2.2
2.0
1.8
1.4
1.6
MICROCOPY RESOLUTION TEST CHART
NATIONAL BUREAU OF STANDARDS-1963-A

ROBUST CONTROL OF MULTITERMINAL DC/AC SYSTEMS*

by

N.A. Lehtomaki, S.M. Chan, N.R. Sandell, Jr., M. Athans, J. Carrig
Laboratory for Information and Decision Systems
Massachusetts Institute of Technology
Cambridge, Massachusetts 02139

C.E. Grund, F. Nozari, R. Hauth
Electric Utility Systems Engineering Department
General Electric Company
Schenectady, New York 12345

INTRODUCTION

In the past two decades, dc power transmission has provided a viable alternative to ac in special applications such as long-distance, point-to-point transmission, asynchronous connection between power systems of different frequencies, and interconnection of systems via underground and undersea cables. Common to all these applications is the two-terminal dc link which consists of a rectifier and an inverter connected by a dc transmission line. The main advantage of dc transmission lies in its ability to transmit a large block of power, with very little loss, from one part of the network to another without the inherent synchronous and stability limitations of ac systems. Although most dc links to date are built for the purpose of bulk-power transmission, it was discovered recently that by modulating the dc current, a dc link can be used as an extremely effective control element for damping some of the inter-area, electromechanical oscillations in an integrated ac/dc system.

The successful application of two terminal dc links suggests that even greater flexibility in power dispatch and enhancement in stability can be realized by a multiterminal dc (MTDC) system embedded in an interconnected ac grid. Several utilities are looking into the possibility of building MTDC systems by adding new terminals to the existing dc links or by connecting dc links that are located in close proximity. It is quite conceivable that MTDC will become a major part of our energy delivery system by the end of this century.

A parallel connected MTDC system is envisaged as a network of n (n>2) inverters and rectifiers interconnected by dc transmission lines. In the steady state, n-1 converters are operated under a constant-current mode, and the nth converter with the lowest ac commutating voltage (voltage that is applied to the ac side of a converter) is operated under constant delay-angle or constant extinction-angle mode and determines the voltage of the entire MTDC system. In a transient condition the terminals of an MTDC system can potentially be modulated in a coordinated manner to damp out the inter-area electromechanical oscillations.

The design of the MTDC control system offers a unique challenge; since it involves a large-scale, multivariable system where the sensors and actuators are situated far apart, and the parameters of the system are difficult to estimate and may change abruptly due to failures such as short circuits or generators outages. A workable design for such a system must be sufficiently robust to tolerate actuator and sensor failures, unmodelled dynamics, and changes in system parameters. Moreover, economic and reliability considerations dictate that some form of decentralized feedback scheme be used, if possible.

* Research supported by the U.S. Department of Energy under contract ET-78-C-01-3395

The intent of this paper is to illustrate how the MTDC control problem can be analyzed from a physical viewpoint, and how the physical insights can be utilized to arrive at a reasonable, robust control design. The main emphasis is on robustness. Some of the latest results in robustness theory are used in the design stage as well as in analyzing the final design.

Although this paper presents a general design methodology for an MTDC system, a hypothetical, five-terminal dc/ac system is used as an example to illustrate the steps of the design process. The model of this system is described in Section I, and a physical interpretation of the design model from a modal perspective is given in Section II. Section III shows how the physical insights can be used to construct a state penalty matrix for an LQ design, and the concept of gain observability is utilized to study the trade-off between the LQ centralized design and other decentralized schemes. The robustness of the control design is studied in Section IV, after a brief review of a relevant theorem in robustness theory. Finally, some results of the open- and closed-loop systems are compared in Section V.

I. MODELLING

The power system being studied consists of an n-terminal MTDC system embedded in an ac system with m groups of coherent machines, each of which is represented by the classical constant-voltage-behind-transient-reactance generator model. For each generator the electrical angle δ is governed by Newton's Second Law for a rotating mass:

$$J\ddot{\delta} + D\dot{\delta} = P_m - P_e \qquad (1)$$

where

- J is a constant related to the inertia of the generator,
- P_m is the mechanical power supplied by the prime mover,
- P_e is the electrical power injected into the power network, and
- D is a constant related to the damping of the machine.

It is further assumed that the mechanical power remains constant over the time period of interest.

The dynamics of the dc converter and the dc network are ignored, because they are much faster than the electromechanical dynamics being studied. If the dc terminals are viewed as actuators, this implies that the control action is equal to the command at all time.

Under these assumptions, a linearized model is obtained by first solving for the steady-state solution of the ac/dc system, and then linearizing the equations about the steady-state point. The result is a linear time-invariant model of the form

$$\dot{\underline{x}}(t) = A\underline{x}(t) + B\underline{u}(t) \qquad (2)$$

where

$\underline{x} \triangleq (\Delta\delta_1, \Delta\omega_1, \ldots, \Delta\delta_m, \Delta\omega_m)^T$ are the changes in electrical angle and frequency of the m generators,

$\underline{u} \triangleq (\Delta I_2, \ldots, \Delta I_n)^T$ are the changes in current injected by the dc terminals.

(The current injection of the first dc terminal is not a control variable). A and B are matrices of appropriate dimension.

In the subsequent discussion, the "Δ" symbol will be dropped, and all quantities are deviations from the steady-state solution unless otherwise specified. It is important to emphasize that the design model (2) does not take into account the dynamics associated with the excitation system, power-system stabilizer, shaft torsional vibrations, and a host of other physical phenomena which are significant at frequencies greater than 30 rad/sec; thus the design model (2) is valid only for low frequencies. This fact will be important when designing the feedback system.

For the purpose of illustration, a hypothetical ac/dc system shown in Figure 1 is used throughout. A physical interpretation of the dynamics associated with this system will be given after a brief discussion on the methods of modal analysis.

II. CONTROLLABILITY, OBSERVABILITY AND PHYSICAL INTERPRETATION OF MODES

Since the linearized model on which the control design is based has limitations, as all models do, it is important to be able to physically interpret the system modes in order that the control system design may be evaluated in part by how it affects them. It is also important to assess beforehand the inherent ability of the available control inputs to accomplish the performance objective using only information furnished by the available output measurements. This is done by computing the open-loop system eigenvalues the corresponding left and right eigenvectors, determining what each mode physically represents and then determining the controllability and observability of each mode.

Modal Analysis

To facilitate the subsequent discussion on the physical interpretation of the system modes the role of the left and right eigenvectors of the system matrix A is reviewed. Consider the open-loop system

$$\dot{\underline{x}}(t) = A\underline{x}(t) \; ; \quad \underline{x}(0) = \underline{x}_0 \qquad (3)$$

where the eigenvalues of A, $\lambda_1, \lambda_2, \ldots, \lambda_n$, are assumed to be distinct. Let $\underline{v}_i$ and $\underline{w}_i^T$ be the right and left eigenvectors respectively of A associated with the eigenvalue λ_i and define the matrices

$$V \triangleq [\underline{v}_1, \underline{v}_2, \ldots, \underline{v}_n] \qquad (4)$$

$$W \triangleq [\underline{w}_1, \underline{w}_2, \ldots, \underline{w}_n]^T = V^{-1} . \qquad (5)$$

The reason for the adjective "right" and "left" is obvious by noting that

$$AV = V\Lambda \qquad (6)$$

$$WA = \Lambda W \qquad (7)$$

where

$$\Lambda \triangleq \mathrm{diag}[\lambda_1, \lambda_2, \ldots, \lambda_n] . \qquad (8)$$

Using the right and left eigenvectors, the matrices A and e^{At} may be written as dyadic expansions:

$$A = \sum_{i=1}^{n} \lambda_i \underline{v}_i \underline{w}_i^T \qquad (9)$$

$$e^{At} = \sum_{i=1}^{n} e^{\lambda_i t} \underline{v}_i \underline{w}_i^T \qquad (10)$$

The unforced response of the system is now given by

$$\underline{x}(t) = \sum_{i=1}^{n} (e^{\lambda_i t} \underline{v}_i)(\underline{w}_i^T \underline{x}_0) \qquad (11)$$

which shows that $\underline{x}(t)$ is simply a linear combination of n time-varying vectors, $e^{\lambda_i t} \underline{v}_i$, or modes each weighted by the scalar $\underline{w}_i^T \underline{x}_0$. A physical interpretation of a right eigenvector, $\underline{v}_i$, can best be illustrated graphically on an Argand diagram where the components of $\underline{v}_i$ are plotted as vectors in the complex plane. The quantity $e^{\lambda_i t} \underline{v}_i$ can be visualized as rotating all components of $\underline{v}_i$ at the same rate $\mathrm{Im}[\lambda_i]$ and simultaneously shrinking or expanding them at the rate $\exp\{\mathrm{Re}[\lambda_i t]\}$ depending on whether λ_i is stable or unstable. This is similar to the phasor representation of sinusoidal signals and is depicted in Figure 2.

The left eigenvectors, on the other hand, determine a linear combination of states that oscillate at the complex frequency equal to the corresponding eigenvalue since

$$\frac{d}{dt}\{\underline{w}_i^T \underline{x}(t)\} = \underline{w}_i^T A\underline{x}(t) = \lambda_i \{\underline{w}_i^T \underline{x}(t)\} . \qquad (12)$$

Physical Interpretation of System Modes

The open-loop eigenvalues of the system are plotted in Figure 3. The Argand diagram associated with each of the four pairs of complex eigenvalues reveals that the frequencies of certain areas are approximately 180° out of phase with that of the other areas. This is interpreted as an electromechanical oscillation in which two coherent groups of areas for a given mode swing against each other. For example, in Figure 4 for the $-.094 \pm j3.80$ modes, the areas 1 and 2 swing against areas 3,4 and 5 with areas 2 and 5 being dominant in the oscillation. The two remaining eigenvalues are real. For the eigenvalue at zero the right eigenvector is

$$\underline{v}_0^T = [1,0,1,0,1,0,1,0,1,0] \qquad (13)$$

where the 1's correspond to angle states and the 0's to frequency states. The physical interpretation is that an arbitrary phase reference exists for this

$$A\underline{x} = A(\underline{x} + \beta\underline{v}_0) \quad . \tag{14}$$

In other words, only the difference in angle states is important since any constant may be added to all the angle states without affecting the dynamic response of the system. The left eigenvector for the remaining mode at -.18 has the form

$$\underline{w}_a^T = [0,H_1,0,H_2,0,H_3,0,H_4,0,H_5] \tag{15}$$

where H_i is the intertia of area i divided by the total system intertia. Equation (12) implies that

$$\dot{\bar{\omega}}(t) = -.18\bar{\omega}(t) \tag{16}$$

where

$$\bar{\omega}(t) \triangleq \underline{w}_a^T \underline{x}(t) = \sum_{i=1}^{5} H_i\omega_i \tag{17}$$

is interpreted as the average frequency of the power system.

The foregoing analysis, clearly demonstrates the role of the left and right eigenvectors in determining the physical interpretation which may not be immediately apparent for some of the system eigenvalues. The left and right eigenvectors are also very useful in determining the controllability and observability of the modes.

Modal Controllability and Observability

Consider the linear system with m inputs, p outputs and n states

$$\dot{\underline{x}}(t) = A\underline{x}(t) + B\underline{u}(t), \quad \underline{x}(0) = \underline{x}_0 \tag{18}$$

$$\underline{y}(t) = C\underline{x}(t) \quad . \tag{19}$$

Using the variation of constants formula gives

$$\underline{x}(t) = e^{At}\underline{x}_0 + \int_0^t e^{A(t-\tau)}B\underline{u}(\tau)d\tau \tag{20}$$

$$\underline{y}(t) = Ce^{At}\underline{x}_0 + \int_0^t Ce^{A(t-\tau)}B\underline{u}(\tau)d\tau \quad . \tag{21}$$

For linear operators $L(\cdot)$ and $H(\cdot)$ let $R(L)$ denote the range of $L(\cdot)$ and $N(H)$ denote the nullspace of $H(\cdot)$. The system defined in (18) and (19) is completely controllable if and only if

$$R(L) = R^n \tag{22}$$

where

$$L(\underline{u}) \triangleq \int_0^t e^{A(t-\tau)}B\underline{u}(\tau)d\tau \tag{23}$$

and is completely observable if and only if

$$N(H) = \{\underline{0}\} \tag{24}$$

where

$$H(\underline{x}_0) \triangleq Ce^{At}\underline{x}_0 \quad . \tag{25}$$

if the state of the system can be driven anywhere in R^n by some control $\underline{u}(\tau)$ applied from $\tau=0$ to t. Analogously, (24) implies that given the output $\underline{y}(t)$ and the input $\underline{u}(\tau)$ for $0\leq\tau\leq t$, the initial state, and thus the state trajectory, can be determined or observed.

There are different ways of determining whether the conditions (22) and (24) are satisfied. However, the definitions of controllability and observability specified in these conditions are qualitative concepts and do not provide quantitative measures of how controllable or how observable a system may be; they can only say what part of the system is controllable or observable and what part is not. Part of the problem is that it is not immediately apparent what is meant by terms like "strongly controllable" or "almost observable", since it is possible to define them differently depending on their intended use.

One possible way to quantify controllability and observability is to measure the change with respect to perturbations in the nominal system model. In other words, if "small" perturbations in the nominal system change, the controllability of certain states, those states would be considered "weakly controllable" or "almost uncontrollable."

A different but not unrelated way of measuring the controllability and observability is based on the intuitive idea of how strongly the modes can be excited by the inputs and how strongly the modes appear at the outputs, respectively. This is made more precise by considering the original qualitative definitions of controllability and observability in terms of the modes of the system. Consider $L(u)$ and $H(\underline{x}_0)$ in terms of the dyadic expansion for $\exp(At)$:

$$L(\underline{u}) = \sum_{i=1}^{n}\left[e^{\lambda_i t}\underline{v}_i\right]\left[\underline{w}_i^T B\right]\int_0^t e^{-\lambda_i\tau}\underline{u}(\tau)d\tau \tag{26}$$

$$H(\underline{x}_0) = \sum_{i=1}^{n}\left[\underline{w}_i^T\underline{x}_0 e^{\lambda_i t}\right]\left[C\underline{v}_i\right] \quad . \tag{27}$$

From (26) it is clear that if $\underline{w}_i^T B=0$ for some i, then $L(\underline{u})$ is a linear combination of at most n-1 eigenvectors for any $\underline{u}$; hence dim $R(L)< n$ and the system is not completely controllable. Similarly from (27), if $C\underline{v}_i=0$ for some i, then $H(\underline{v}_i)=0$ but $\underline{v}_i\neq 0$; hence dim $N(H)> 0$ and the system is not completely observable. These facts are immediately obvious once $\underline{y}(t)$ is written as

$$\underline{y}(t) = \sum_{i=1}^{n} C\underline{v}_i\left[\underline{w}_i^T\underline{x}_0 + \underline{w}_i^T B\int_0^t e^{-\lambda_i\tau}\underline{u}(\tau)d\tau\right]e^{\lambda_i t} \quad . \tag{28}$$

If $\underline{w}_i^T B=0$ then the input $\underline{u}$ cannot excite the $i^{\underline{th}}$ mode and if $C\underline{v}_i=0$ the $i^{\underline{th}}$ mode does not appear in the output $\underline{y}(t)$. In these cases the $i^{\underline{th}}$ mode is said to be uncontrollable or unobservable respectively. If the matrices B and C are given by

$$B = [\underline{b}_1,\underline{b}_2,\ldots,\underline{b}_m] \tag{29}$$

$$C = [\underline{c}_1,\underline{c}_2,\ldots,\underline{c}_p]^T \tag{30}$$

where $\underline{b}_i$ is the $i^{\underline{th}}$ column of B and $\underline{c}_i^T$ is the $i^{\underline{th}}$ row of C then the matrices WB and CV given by

$$WB = \begin{bmatrix} \underline{w}_1^T\underline{b}_1 & \underline{w}_1^T\underline{b}_2 & \cdots\cdots & \underline{w}_1^T\underline{b}_m \\ \underline{w}_2^T\underline{b}_1 & \underline{w}_2^T\underline{b}_2 & \cdots\cdots & \underline{w}_2^T\underline{b}_m \\ \vdots & \vdots & & \vdots \\ \underline{w}_n^T\underline{b}_1 & \underline{w}_n^T\underline{b}_2 & \cdots\cdots & \underline{w}_n^T\underline{b}_m \end{bmatrix} \tag{31}$$

and

$$CV = \begin{bmatrix} \underline{c}_1^T\underline{v}_1 & \underline{c}_1^T\underline{v}_2 & \cdots\cdots & \underline{c}_1^T\underline{v}_n \\ \underline{c}_2^T\underline{v}_1 & \underline{c}_2^T\underline{v}_2 & \cdots\cdots & \underline{c}_2^T\underline{v}_n \\ \vdots & \vdots & & \vdots \\ \underline{c}_p^T\underline{v}_1 & \underline{c}_p^T\underline{v}_2 & \cdots\cdots & \underline{c}_p^T\underline{v}_n \end{bmatrix}, \tag{32}$$

have a nice interpretation: the magnitude of the entry $\underline{w}_i^T\underline{b}_j$ of WB measures how much the j^{th} input of $\underline{u}$ affects the i^{th} mode and the magnitude of the entry $\underline{c}_i^T\underline{v}_j$ of CV measures how much the j^{th} mode appears in the i^{th} output of $\underline{y}(t)$.

If the rows of C and the columns of V are normalized to have unit euclidean length, the magnitude of $\underline{c}_i^T\underline{v}_k$ represents the cosine of the angle between the vectors $\underline{c}_i$ and $\underline{v}_k$. Thus when $\underline{c}_i$ and $\underline{v}_k$ are nearly orthogonal the k^{th} mode is unobservable from the i^{th} output for some small perturbations of the nominal system.

In interpreting (31) and (32), it is important to keep in mind that the magnitude of $||\underline{w}_i^T\underline{b}_j||$ and $||\underline{c}_i^T\underline{v}_j||$ depends on the choice of units of the input and output as well as the scaling of the eigenvectors. If the units of the input and output are considered fixed, the quantity $||C\underline{v}_i||$ can only be made large by making $||\underline{w}_i^TB||$ small, since $V=W^{-1}$ and $\underline{w}_i^T\underline{v}_j = \delta_{ij}$. Thus it seems reasonable to balance the left and right eigenvectors corresponding to the same eigenvalue by making their norms equal. This ensures that a mode does not appear very observable but not very controllable or vice versa only because of the scaling chosen. It is also worth noting that the matrix products CV and WB are invariant under similarity transformations of the original system, and the terms $C\underline{v}_i\underline{w}_i^T\underline{x}_0$ and $C\underline{v}_i\underline{w}_i^TB$ in (28) are independent of the scaling of the right and left eigenvectors as long as $W=V^{-1}$. For the power system model, the matrices CV and WB (where the left and right eigenvectors are balanced), have the magnitudes of their elements plotted on bar graphs in Figures 5 and 6. The bars are plotted in pairs, the one on the left for the observability at the indicated output and the one on the right for the controllability at the indicated input. This is done for each mode of the system. In Figure 5 the heights of the bars in a given row have been scaled such that the most controllable and most observable mode for the given input and output have bars of unit height. In Figure 6 the bar heights have been scaled column-wise such that for a given mode the bars of the input and output from which the mode is most controllable and observable have unit height. Notice that the arbitrary phase reference mode is not observable from any frequency output but is controllable from every current input. From both Figures 5 and 6 it is evident that the most observable oscillatory modes in each frequency output are also the most controllable from the input of the same area. This has important ramifications for the control system design in that the sensors and actuators may be colocated, obviating the need for expensive communication links.

III. LINEAR QUADRATIC REGULATOR DESIGN

The basic design methodology adopted here is that of using a linear quadratic regulator to obtain a first iteration centralized design that moves the open loop poles of the system to an appropriate closed loop pole region. This region is determined approximately on engineering judgement by how large the closed loop bandwidth may be made without allowing unmodeled high frequency disturbances or dynamics to destabilize the system. The centralized design is done with an eye towards later decentralization which uses only the measurable frequency states. The decentralized control law then attempts to mimic the centralized control law by including only the important feedback gains from the centralized feedback gain matrix.

Centralized Design

The optimal feedback control law that minimizes the cost functional

$$J(\underline{u}) = \int_0^\infty \underline{x}^T(t)Q\underline{x}(t) + \underline{u}^T(t)R\underline{u}(t); \quad Q\geq 0;\ R>0 \tag{33}$$

is given by the familiar

$$\underline{u}^*(t) = -R^{-1}B^TK\underline{x}(t) \tag{34}$$

where

$$A^TK+KA+Q - KBR^{-1}B^TK = 0 \tag{35}$$

under the usual assumptions that $[A;Q^{1/2}]$ is detectable and [A,B] is stabilizable. The state weighting matrix Q is selected so that neither the real average frequency pole nor the arbitrary phase reference pole at zero are moved. It is not desirable to move the pole at zero since it is only observable from the angle states which are not measurable. The average frequency pole is not to be moved since the load frequency control loop is to control that mode. The only modes that are to be changed are the inter-area oscillatory modes since they require significant damping. There are at least two ways that the state weighting matrix Q may be selected to do this. The first method, a modal one, is more general than the second method which depends on the physical interpretation of the system.

Modal Selection of Q Matrix

Consider the diagonalization of the system (18) by defining a modal vector $\underline{z}(t)$ given by

$$\underline{z}(t) = W\underline{x}(t) \tag{36}$$

which results in

$$\dot{\underline{z}}(t) = \Lambda\underline{z}(t) + WB\underline{u}(t) \tag{37}$$

The basic idea in the selection of Q is to weight only those components of $\underline{z}(t)$ in the cost that correspond to poles of the open-loop system that are to be moved. The rest of the modes of the system are made cost unobservable. Thus, if D is a diagonal matrix of weightings for each mode then (33) becomes

$$J(\underline{u}) = \int_0^\infty ||D\underline{z}(t)||_2^2 + \underline{u}^T(t)R\underline{u}(t)dt \quad , \qquad (38)$$

Note that the term $||D\underline{z}(t)||_2^2$ can be converted into $\underline{x}^T(t)Q\underline{x}(t)$ with a real Q matrix in the following way. Define Γ as

$$\Gamma = DW = \Gamma_R + j\Gamma_I \qquad (39)$$

then

$$||D\underline{z}(t)||_2^2 = \underline{x}^T(t)W^H D^2 W\underline{x}(t) = \underline{x}^T(t)Q\underline{x}(t) \qquad (40)$$

where

$$Q = \Gamma_R^T \Gamma_R + \Gamma_I^T \Gamma_I \qquad (41)$$

There is a slight difficulty with this method, however, in that $[A,Q^{1/2}]$ may not be detectable. This is the case because the arbitrary phase reference mode at zero is made cost unobservable. One way around this problem is to use a reduced model that does not have this mode. An alternative way is to artificially stabilize the cost unobservable unstable modes leaving the other system modes fixed. This new system is essentially the same as the old system for the purposes of design of a feedback controller since the controller will not attempt to stabilize the unstable cost unobservable modes. This is accomplished utilizing the dyadic expansion of the A matrix in (9). Let $\tilde{A}$ be the artificially stabilized system matrix which is defined by

$$\tilde{A} = \sum_{i \notin \Omega} \lambda_i \underline{v}_i \underline{w}_i^T - \epsilon \sum_{i \in \Omega} \underline{v}_i \underline{w}_i^T \quad ; \quad \epsilon > 0 \qquad (42)$$

where

$$\Omega \triangleq \{i: \lambda_i \text{ mode is unstable and cost unobservable}\} \ , \qquad (43)$$

Now the matrix $\tilde{A}$ has the same eigenvectors as A and the same eigenvalues as A except for those associated with the index set Ω. This ensures that the old and new system will behave the similarly from the standpoint of controller design. A somewhat simpler variation of this approach, which works if ϵ is sufficiently small, is to define $\tilde{A}$ as $\tilde{A}=A-\epsilon I$. Then $\tilde{A}$ has the same eigenvectors as A and eigenvalues ϵ away from those of A.

Average Frequency Deviation Selection of Q Matrix

The second method of selecting the state weighting matrix Q is to weight only each machine's or area's frequency deviation from the average frequency. Thus the state weighting is

$$\underline{x}^T(t)Q\underline{x}(t) \triangleq \sum_{i=1}^{5} \alpha_i (\omega_i - \bar{\omega})^2 \qquad (44)$$

where α_i is the i^{th} average frequency deviation weighting for the i^{th} area. This Q only weights frequency variables so that the zero pole will not be moved and since only deviations from the average frequency are weighted the average frequency is used as a reference and hence the pole at -.18 will not be moved. Using this method also requires the stabilization of the zero phase reference mode. Therefore in the centralized design, ϵI is subtracted from the system A matrix and is used as the system matrix when solving the Riccati equation (35); the resulting feedback control, however, is applied to the original unstabilized system. Both methods of selecting Q require only a few iterations of selecting modal weightings or frequency deviation weightings to obtain the approximate damping of the oscillatory modes required. It is interesting that both methods give approximately the same feedback gains. The centralized design that is used throughout the remainder of the paper is based on the weighting of deviations from average frequency. It should also be mentioned that the control weighting matrix R was selected as the identity matrix multiplied by a scalar to tradeoff state and control energy.

Feedback Structures

In order to describe several controllers that result from modifications of the centralized controller it is necessary to classify several different feedback structures. They are the following:

(1) LQ Centralized - full state feedback

(2) LQ Full State without Angles - frequency feedback only

(3) LQ Major - local area frequency and frequency of area 1 available for feedback (the major centralized gains)

(4) LQ Decentralized - only local areafrequency available for feedback.

In each case the feedback gain for the controller structure is obtained by simply setting the gains in the centralized gain matrix, that correspond to states not available for feedback, to zero. The closed-loop eigenvalues for cases 1, 3 and 4 are given in Figure 7. To assess how closely each of the feedback controllers mimic the centralized feedback controller the concept of gain observability is introduced.

Gain Observability

The ability to realize a centralized feedback law in a decentralized manner depends critically on the nature of the centralized feedback law. It may not even be possible if the centralized feedback law depends substantially on states not available for feedback. Thus only modes observable from the frequency outputs are moved in the centralized design. Eliminating gains in the centralized gain matrix that do not significantly affect the feedback is commonly done by setting the "small" gains to zero. What is considered "small" must be considered in reference to the expected size of the variations in the state. However, it is not always clear what the expected variations are since, in general, some of the state variables may not be physical quantities. Also, while a particular gain may not by itself be insignificant, a group of certain gains may collectively have very little effect on the feedback control signal implemented since cancellation of the contributions of different gain-state products may occur when summed. This later idea is made precise by the notion of gain observability. Gain observability merely determines

the modes being fedback in each control channel by using the gain matrix as an output measurement matrix and computing the matrix GV where G is the gain matrix and V, given by (4), is the matrix of right eigenvectors. By computing GV for different gain matrices G, the modas being fedback in each channel may be compared. This is done in Figure 8 for che four feedback structures previously described. From Figure 8 it is apparent that the LQ Centralized and LQ Full State without Angle feedback cases are practically identical indicating it is not important to try and measure the angle states. The LQ Major case is also quite similar to the LQ Centralized case while the LQ Decentralized case is somewhat less so. Thus gain observability indicates the dominant modes in each feedback channel and provides insight on how to construct a decentralized or limited state feedback controller that approximates a centralized controller.

As a matter of practical importance, each control signal in the real system is passed through a washout which washes out any constant frequency errors that may be generated. The washouts have a transfer function $\frac{s}{s+.2}$ and are included in the subsequent analysis as part of the controllers.

IV. ROBUSTNESS

In any control system design there is a degree of uncertainty about the model parameters and about the nature of the disturbances that act as exogenous inputs to the model. A well designed control system must be able to tolerate such uncertainty without destabilizing the system. Classically, a measure of robustness has been the notions of gain and phase margin for SISO feedback systems. In the multivariable version of the Nyquist stability theorem, the gain and phase margins do not provide an adequate measure of the robustness of the nominal feedback system since arbitrarily small simultaneous perturbations in the nominal system may cause instability of the closed-loop system even though there are good gain and phase margins in each feedback channel.

The multivariable Nyquist criterion counts the encirclements of the origin by the det(I+G(jω)) where G(s) is the loop transfer functions. In order to change the number of encirclements of the origin, det(I+G(jω)) must be zero for some ω. Thus for nominally stable closed-loop systems the det(I+G) tries to measure the "distance" of I+G to the critical point but is not a good measure because det(I+G) may be very sensitive to small changes in G. In the scalar case det(I+G) becomes 1+g and small changes in g yield only small changes in the Nyquist diagram of 1+g or g so that this problem does not arise. Therefore, in the multivariable setting what is required is an insensitive measure of the "distance" of I+G to the origin. The minimum singular value of I+G is such a measure. It measures the minimum size of the additive perturbation, ΔG, required to make det(I+G+ΔG)=0 or I+G+ΔG exactly singular. The minimum and maximum singular values are denoted as $\underline{\sigma}$ and $\bar{\sigma}$ respectively and are defined by

$$\underline{\sigma}(A) \triangleq \min_{x\neq 0} \frac{||Ax||_2}{||x||_2} = \frac{1}{||A^{-1}||_2}, \text{ if } A^{-1} \text{ exists} \tag{45}$$

$$\bar{\sigma}(A) \triangleq \max_{x\neq 0} \frac{||Ax||_2}{||x||_2} \triangleq ||A||_2 \tag{46}$$

Therefore if at some frequency ω_0, $\underline{\sigma}(I+G(j\omega))$ is small, there exists a small perturbation in the nominal system that will make the closed-loop system unstable. It has been known for some time that linear quadratic regulators for single input-single output systems have inherently good, guaranteed gain and phase margins, of namely infinite upward and 50% reduction gain margins and ±60° phase margin [1]. This is because for LQ regulators $|1+g(j\omega)| \geq 1$ $\forall\omega$ so that the Nyquist diagram of g must avoid the unit disk centered at (-1,0). This is shown in Figure 9. For multivariable systems, Kalman's well-known inequality for LQ regulators [3,4] generalizes with R=I to

$$(I+G(-s))^T(I+G(s)) \geq I \qquad \forall s \tag{47}$$

so that

$$\underline{\sigma}(I+G(j\omega)) \geq 1 \qquad \forall\omega \tag{48}$$

is analogous to the scalar case where $|1+g(j\omega))| \geq 1$. It has more recently been shown [2] that for diagonal R>0 and Q>0 that the multivariable LQ regulators have the same gain and phase margins in each feedback channel simultaneously as in the single input-single output case. However, as is well known, the infinite gain margin is not a reality for the real world because the nominal model is only valid within a limited frequency range and furthermore a constant feedback gain at all frequencies is not realizable. Thus the bandwidth of the closed loop system must still be checked to ensure that the bandwidth is not excessive and that the loop is rolled off sufficiently where unmodelled dynamics might affect the closed loop stability of the system. The following robustness theorem checks this in a more formal way.

Robustness Theorem [5,6]:

Let $\tilde{G}(s)$ be the transfer function matrix of a proper finite dimensional linear system. Let G(s) be its nominal (design) value, also proper and let $\Delta G_A(s)$ and $\Delta G_M(s)$, defined by the relations,

$$\tilde{G}(s) \triangleq G(s) + \Delta G_A(s) \tag{49}$$

$$\tilde{G}(s) \triangleq (I+\Delta G_M(s))G(s) \tag{50}$$

be such that $\tilde{G}(s)$ and G(s) have the same number of open-loop poles in the closed right half plane. If the nominal feedback system

$$G(s)[I+G(s)]^{-1} = (I+G^{-1}(s))^{-1} \tag{51}$$

is stable, then the perturbed system

$$\tilde{G}(s)[I+\tilde{G}(s)]^{-1} \tag{52}$$

is stable for all perturbations satisfying

$$\underline{\sigma}(I+G(j\omega)) > \bar{\sigma}(\Delta G_A(j\omega)) \qquad \forall\omega \tag{53}$$

or

$$\underline{\sigma}(I+G^{-1}(j\omega)) > \bar{\sigma}(\Delta G_M(j\omega)) \qquad \forall\omega \ . \tag{54}$$

Alternatively, the conditions (53) and (54) may be replaced by (55) and (56) respectively given as

$$||(I+G(j\omega))^{-1}||^{-1} > ||\Delta G_A(j\omega)|| \qquad \forall\omega \tag{55}$$

$$||(I+G^{-1}(j\omega))^{-1}||^{-1} > ||\Delta G_M(j\omega)|| \qquad \forall\omega \tag{56}$$

where $||\cdot||$ denotes the 1 or ∞ matrix norms. □

Computationally, $\|\cdot\|_1$ or $\|\cdot\|_\infty$ are cheaper and easier to compute than $\sigma(\cdot)$ and thus are used in the subsequent discussion in place of the singular values[7].

To test the robustness of the modified LQ controller for the multiterminal dc system, several plots of the norms specified in conditions (55) and (56) have been computed with respect to different perturbed models. The nominal model consists of the open-loop system regulated by the LQ major controller modified, as previously described, by passing the control inputs through washouts with transfer function

$\frac{s}{s+.2}$ to eliminate response to constant frequency errors. The perturbed model is the same as the nominal except that it includes additional filtering of the control inputs by an approximately unity gain double pole filter at s=25 to simulate the additional phase lag of torsional filters in the real system. The plot for the multiplicative perturbation, Figure 11, shows that the perturbed system is stable and that the nominal system has a degree of robustness even beyond the perturbation. It is interesting to note that the additive perturbation, Figure 10, for the same perturbed model exceeds the nominal at the system resonances. This points out the fact that the conditions (55) and (56) are only sufficient but not necessary. Here in lies one of the major weaknesses of the singular value approach; it is sometimes unnecessarily conservative. In Figures 12 and 13 the LQ Major controller is checked for robustness with respect to a perturbed system that includes an additional machine, with relatively small inertia, that is weakly coupled to the rest of the system to model intra-area dynamics. The resulting changes in the closed-loop system eigenvalues are insignificant even though the sufficient conditions indicate there does exist a perturbation of the same size as the additional intra-area dynamics that will destabilize the system. Notice also in the Figures 10 and 11 that $\|(I+G)^{-1}\|^{-1}$ and $\|(I+G^{-1})^{-1}\|^{-1}$ do not become small at any frequency which is indicative of robustness.

To make the connection with the classical SISO gain and phase margins, under the LQ major controller with washouts, one of the system feedback loops is broken. The margins for this channel are an infinite upward gain margin, a gain reduction margin of 100% and a phase margin of $\pm$100 degrees. This also gives an indication of how conservative the norm plots may be, since they take into account perturbations in the system that may not be reasonable. Other robustness norm-plots for the completely centralized decentralized case are similar in nature. The centralized case has the largest $\|(I+G)^{-1}\|^{-1}$, as expected, and the decentralized the smallest.

Another method of evaluating the design is to break feedback loops simulating actuator or sensor failure or manual intervention and check the stability of the resulting system. If the system remains stable under the breaking of feedback loops the integrity of the system is said to be maintained. Even though a system is open-loop stable, this does not guarantee the the closed-loop will remain stable when feedback loops are broken. Thus it is important to check the integrity of the closed-loop system. For the LQ major feedback law with washouts added, the system integrity is maintained for all possible combinations of broken feedback loops. The same is true for the completely decentralized feedback law with washouts also.

Finally, a comparison between the open-and closed-loop bandwidths is made. In Figure 14 $\|G(j\omega)\|$, the maximum open-loop frequency response, and $\|(I+G^{-1}(j\omega))^{-1}\|$, the maximum closed-loop response, are plotted against frequency. This shows that the control law just damps out the resonances in the open-loop system without affecting the rest of frequency response. Control energy is not wasted in modifying the open-loop system more than necessary. This is related to the performance of the control system which is discussed next.

V. CONTROL SYSTEM PERFORMANCE

Evaluation of the closed-loop system performance is done by examining the system transient responses and feedback control inputs to the system generated by an initial condition corresponding to the state vector for the open-loop system after the clearing of a three-phase ground fault at area 4. Figure 15 shows the angle of area 4 using area 3 as a reference (i.e. $\delta_4-\delta_3$) for the open-loop, the LQ centralized, LQ major and LQ decentralized designs with the washouts in place. Figure 16 shows the corresponding frequency ω_4 for the same initial condition and controllers.

As can be seen from these figures, all the controllers give approximately the same performance in the transient responses. They significantly reduce the settling time of the inter-area oscillations. These responses are typical of all the angle and frequency transient responses. However, the control inputs for the various controllers are distinguishable. Figure 17 displays the control signal u_2 for the three different controllers, again with the washouts in place. As can be seen, the centralized feedback gain uses the least control energy indicating a coordinated control effort. The decentralized controller, as expected, use the most since it lacks information to yield a coordinated effort. The effect of the communication of the frequency of area one to all other areas can be assessed in terms of the difference in the control energy for the LQ major and LQ decentralized cases.

VI. SUMMARY

In this paper some of the fundamental concepts of linear system theory are exploited to gain a better understanding of the internal dynamics of the system and how it is related to the external environment. It is shown how the right and left eigenvectors help physically interpret the response of the system at different outputs when excited from different inputs making use of the concepts of modal controllability and observability. A method for selecting the state weighting matrix to relocate only specified modes is given. The concept of gain observability is utilized in comparing different feedback structures, with limited state feedback, with the centralized full state feedback controller. It is seen through simulation that the cost of a decentralized feedback structure is that more control energy is required to damp out oscillations due to the loss of communication of important information. The controllers are shown to be robust with respect to model uncertainty by use of multivariable and classical robustness measures. The integrity of the system is also maintained in the face of all possible actuator or sensor failures. These considerations, that the practicing control engineer must take into account in the design of a practical control system, are illustrated in this design and its evaluation. It is important to emphasize that the multiterminal dc controller design is based on a linearized model and does not consider large signal, nonlinear phenomena such as converter mode switching. These are topics for future research.

REFERENCES

[1] Anderson, B.D.O. and Moore, J.B., Linear Optimal Control, Prentice-Hall, 1971.

[2] Safonov, M.G., and M. Athans, "Gain and Phase Margins for Multiloop LQG Regulators," IEEE Trans. Auto. Control, Vol. AC-22, pp. 173-179, April 1977.

[3] Kalman, R.E., "When is a Linear System Optimal," J. Basic Eng., Trans. ASME, Ser, D. Vol. 86, pp. 51-60, 1964.

[4] Anderson, B.D.O., "The Inverse Problem of Optimal Control," Fourth Annual Allerton Conference on Circuit and System Theory, Urbana, Ill., Oct. 1966.

[5] Doyle, J.C., "Robustness of Multiloop Linear Feedback Systems," IEEE Conf. on Dec. and Control, San Diego, CA., Jan. 1979.

[6] Sandell, Jr., N.R., "Robust Stability of Linear Dynamic Systems with Application to Singular Perturbation Theory," Laboratory for Information and Decision Systems, MIT, Report ESL-P-837, August 1978.

[7] Laub, A.J., "Robust Stability of Linear Systems-Some Computational Considerations," Laboratory for Information and Decision Systems, MIT, Report LIDS-R-904, Feb. 1979.

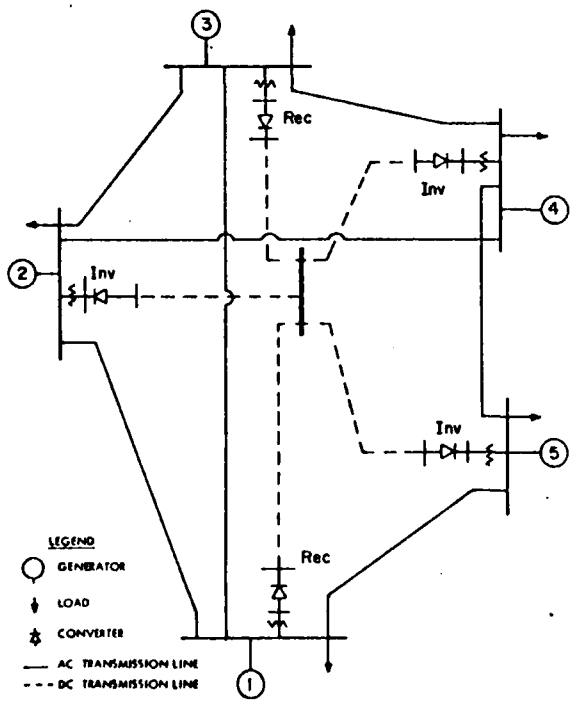

Figure 1: A Power System with 5 DC Terminals and 5 AC Nodes, each representing an Area or Group of Coherent Generators.

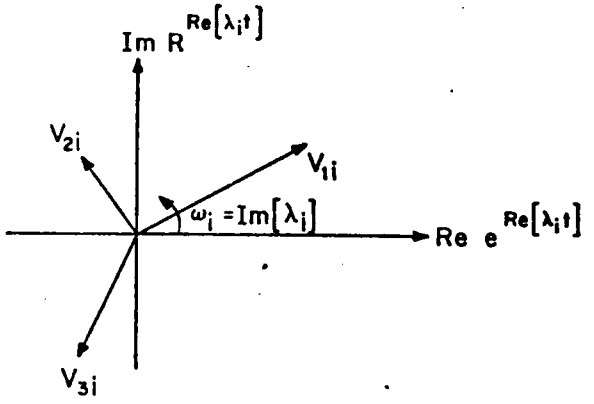

Figure 2: Argand Diagram for $i^{\underline{th}}$ Mode.

Figure 3: Open-Loop Eigenvalues with Nonnegative Imaginary Parts.

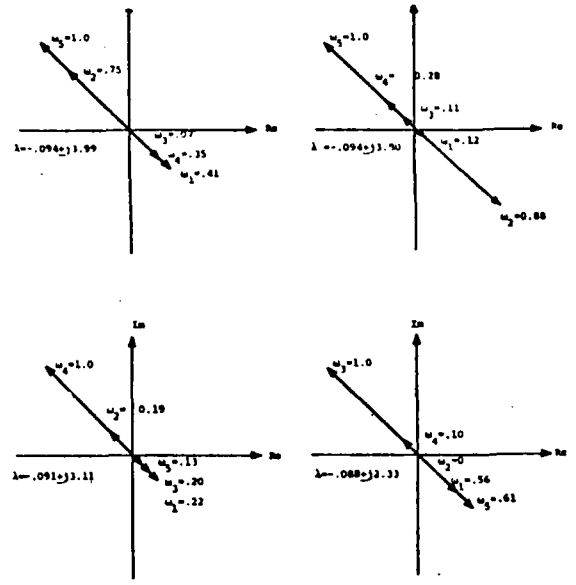

Figure 4: Argand Diagrams of Oscillatory Modes.

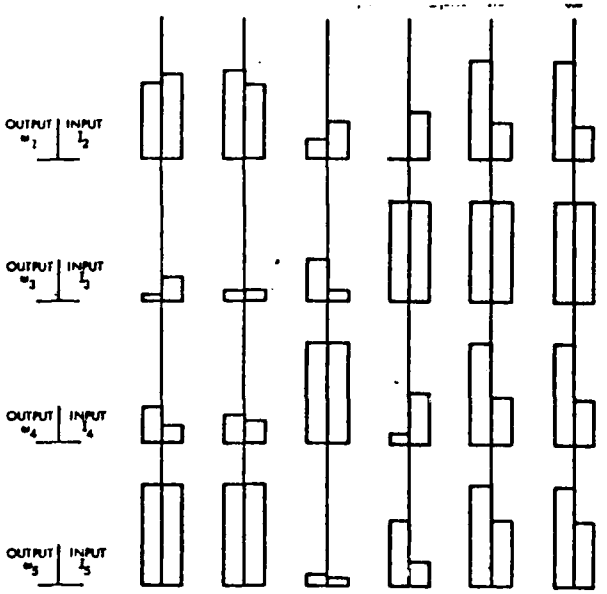

Figure 6: Modal Observability and Controllability of a Specified Mode from Different Inputs or Outputs.

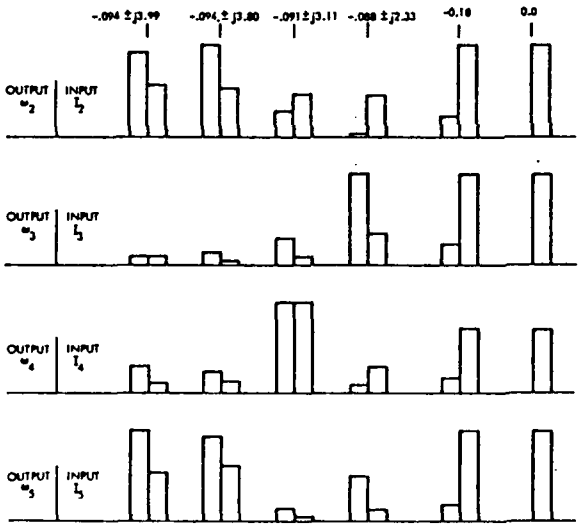

Figure 5: Modal Observability and Controllability of Different Modes from a Specified Input or Output.

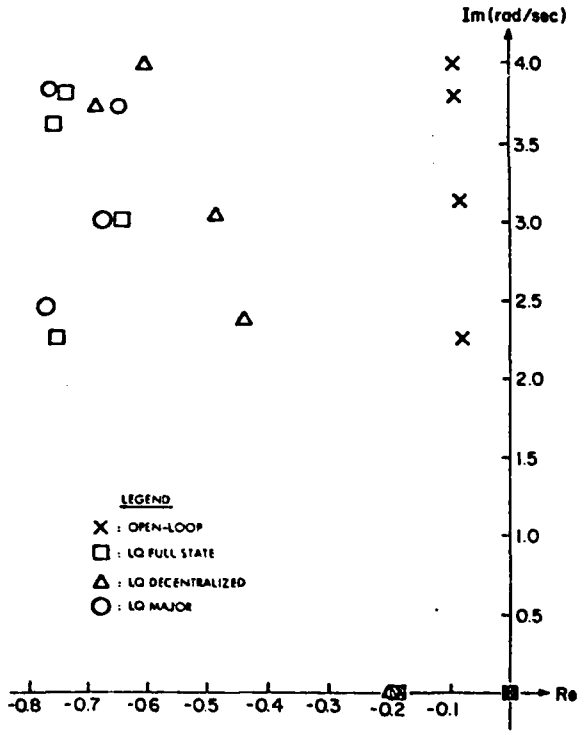

Figure 7: Closed-Loop Eigenvalues for Different Controllers.

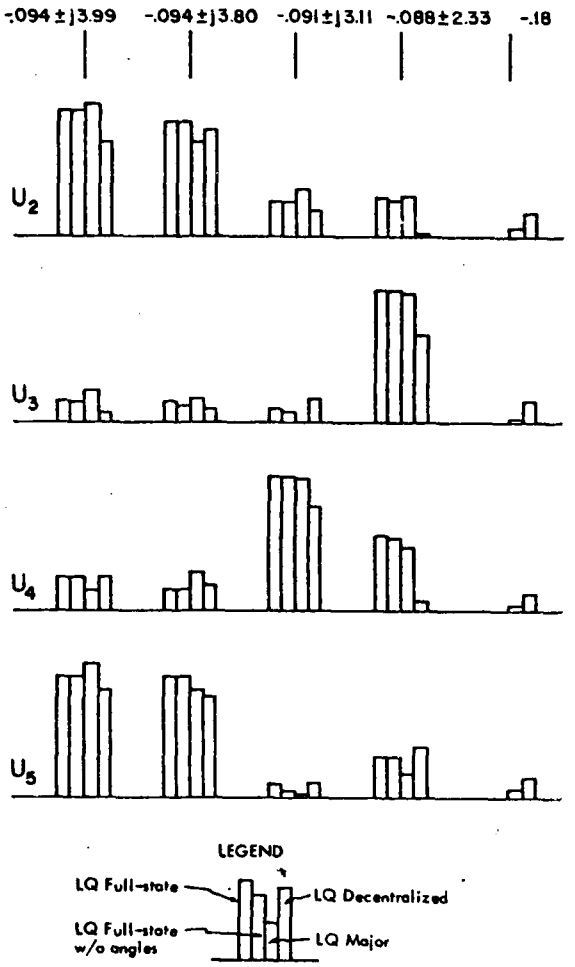

Figure 8: Gain Observability for Different Controllers.

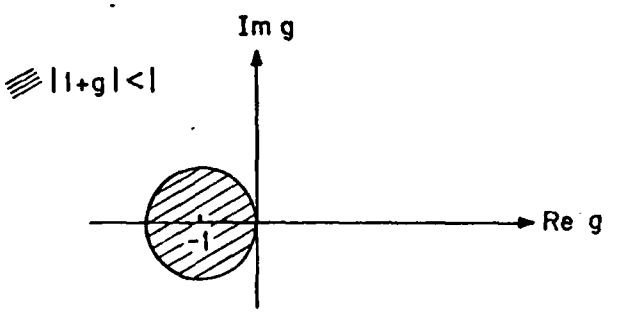

Figure 9: Disk that Nyquist Diagram for SISO LQ Regulator must avoid.

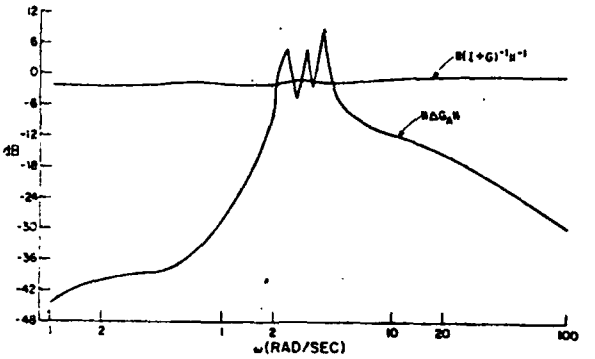

Figure 10: Robustness for Additive Perturbation of Additional Torsional Filters.

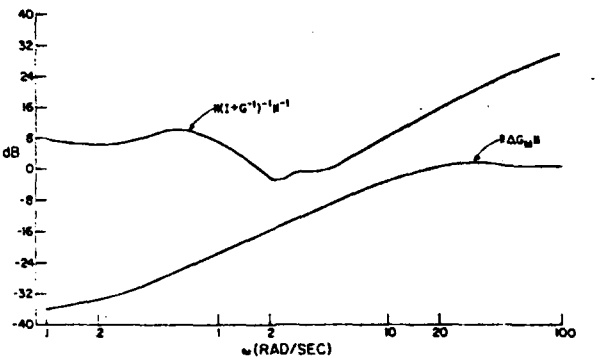

Figure 11: Robustness for Multiplicative Perturbation of Additional Torsional Filters.

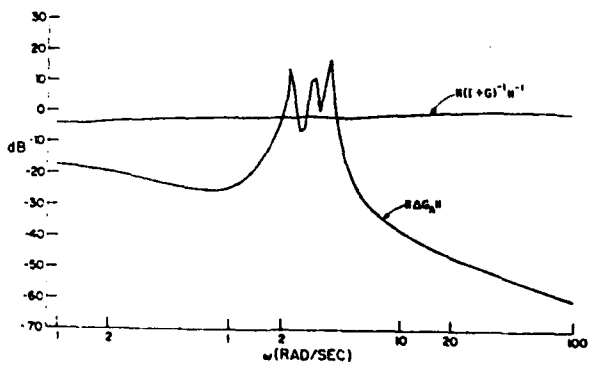

Figure 12: Robustness for Additive Perturbation of Additional Intra-Area Dynamics.

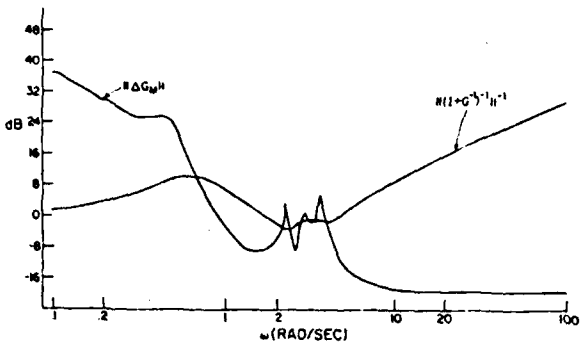

Figure 13: Robustness for Multiplicative Perturbation of Additional Intra-Area Dynamics.

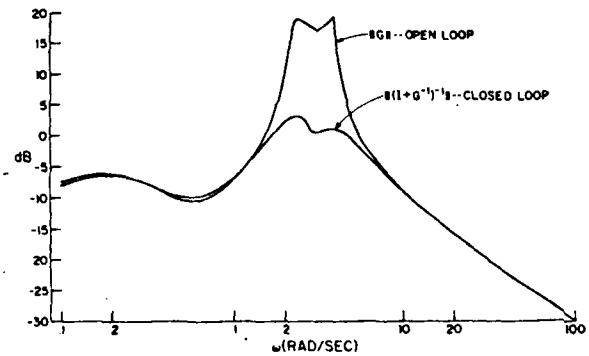

Figure 14: Maximum Open-Loop/Closed-Loop Multivariable Frequency *Response*.

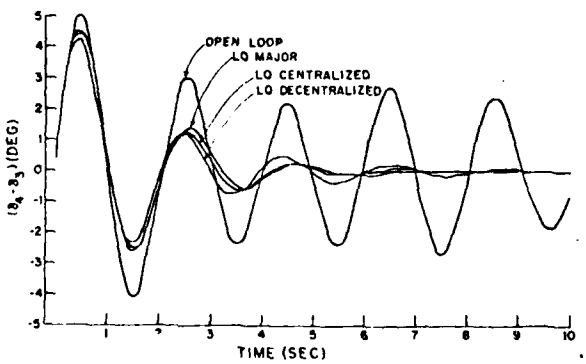

Figure 15: Comparison of $(\delta_4-\delta_3)$ Response for Different Controllers.

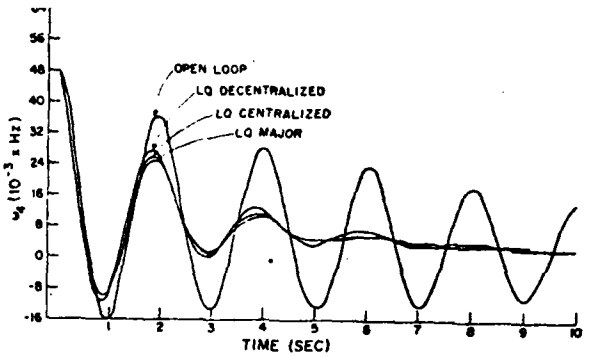

Figure 16: Comparison of ω_4 Response for Different Controllers.

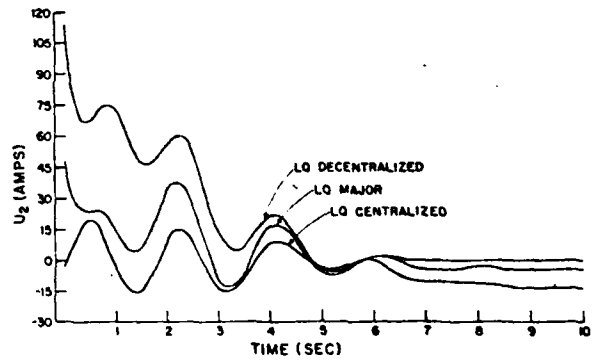

Figure 17: Comparison of u_2 Input for Different Controllers.